pubs.acs.org/cm

Toward High-Voltage Cathodes for Zinc-Ion Batteries: Discovery **Pipeline and Material Design Rules**

Roberta Pascazio, Qian Chen, Haoming Howard Li, Aaron D. Kaplan, and Kristin A. Persson*



Cite This: https://doi.org/10.1021/acs.chemmater.5c00916



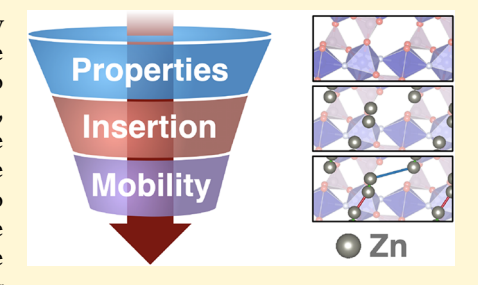
ACCESS I

Metrics & More

Article Recommendations

Supporting Information

ABSTRACT: Efficient energy storage systems are crucial to address the intermittency of renewable energy sources. As multivalent batteries, Zn-ion batteries (ZIBs), while inherently low voltage, offer a promising low-cost alternative to Li-ion batteries due to the viable use of zinc as the anode. However, to maximize the potential impact of ZIBs, rechargeable cathodes with improved Zn diffusion are needed. To better understand the chemical and structural factors influencing Zn-ion mobility within battery electrode materials, we employ a high-throughput computational screening approach to systematically evaluate candidate intercalation hosts for ZIB cathodes, expanding the chemical search space on empty intercalation hosts that do not contain Zn. We leverage a high-throughput screening funnel to identify promising cathodes in ZIBs, integrating



screening criteria with density functional theory (DFT)-based calculations of Zn²⁺ intercalation and diffusion inside the host materials. Using these data, we identify the design principles that favor Zn-ion mobility in candidate cathode materials. Building on previous work on divalent-ion cathodes, this study broadens the chemical space for next-generation multivalent energy storage systems.

■ INTRODUCTION

Downloaded via 67.169.126.188 on August 19, 2025 at 15:40:53 (UTC).
See https://pubs.acs.org/sharingguidelines for options on how to legitimately share published articles.

The interplay between economic development and environmental impact underscores the urgent need for novel sustainable energy sources and, when intermittent renewables fall short of continuous demand, efficient energy storage systems. 1-3

Since their first commercialization by Sony in the 1990s,⁴ lithium-ion batteries (LIBs) have dominated the energy storage market, gradually becoming ubiquitous in portable devices and electric vehicles. 5,6 However, the long-term viability of lithium-ion batteries (LIBs) is hindered by several challenges, including safety risks due to the flammability of commonly used electrolytes, high costs, and the limited availability of critical metals such as cobalt and nickel. 7,8 In response to these challenges, multivalent metal-ion batteries (e.g., Ca²⁺, Mg²⁺, Al³⁺) have been suggested as promising alternative energy storage technologies, leveraging the practical use of metal anodes with liquid electrolytes to achieve low cost and competitive volumetric energy density. 9,10 As an example, zinc-ion batteries (ZIB) have recently gained attention for the attractive properties of the Zn metal anode which offers (i) a high volumetric energy density (5850 mAh/cm³, 10,11 compared to ~2000 mAh/cm³ for LIBs¹²); and (ii) possible utilization in aqueous batteries¹³,14 with notable improvement in their safety, sustainability, and operating costs. 15,16 When coupled with the appropriate choice of working conditions (e.g., pH) and electrolytes, aqueous ZIBs can be optimized to reduce toxicity and increase the reversibility of the plating and stripping of the Zn anode in candidate ZIBs. To increase their voltage window above the limit imposed by water splitting

(~1.23 V), hybrid aqueous-nonaqueous solvents¹⁷⁻²⁰ building on water-in-salt electrolytes (WISE) and 21 alternative water-in-organic strategies^{22,23} have shown an improvement, effectively suppressing water decomposition and proton intercalation and enabling operational windows of up to ~1.6 V vs Zn/Zn²⁺. Polymer-based^{24,25} and ionic liquid²⁶based electrolytes have also been investigated for ZIBs, identifying the formation of Zn dendrites as the major limitation to their cycle lives and electrochemical stabilities. Nonaqeuous mixtures of Zn salts and organic solvents have also been examined for their electrochemical and transport properties, as well as their charge-transfer performance at the electrode-electrolyte interface. These electrolyte mixtures, particularly those containing acetonitrile and propylene carbonate, displayed reversible deposition on Zn anodes and wide electrochemical windows (up to 3.8 V vs Zn/Zn^{2+}), suggesting their potential application in ZIBs as electrolytes with a variety of cathode materials.²⁷⁻³⁰

Alongside the advancement of electrolytes, the development of high-performance ZIBs has also been directed toward the positive electrode.³ For instance, a measured capacity of 240 mAh/g at $\sim 1.3 \text{ V vs Zn/Zn}^{2+}$ has been reported for MnO₂, ¹⁰

Received: April 15, 2025 Revised: June 26, 2025 Accepted: June 27, 2025



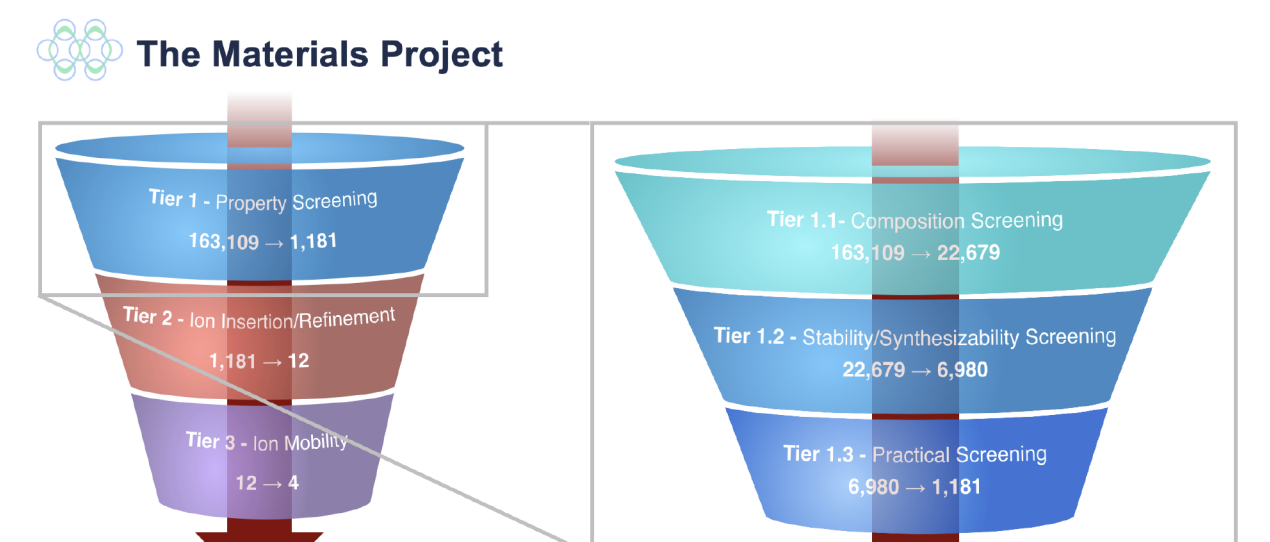


Figure 1. (Left panel) Funnel diagram summarizing the screening process for identifying cathodes for ZIBs from host candidates in the deintercalated state, showing the number of materials entering and exiting each stage. The process is divided into three stages, ordered by increasing computational cost: Tier 1. Materials Project property screening; Tier 2. Ion insertion calculations and additional property screenings/prototype matches; Tier 3. Ion mobility calculations. (Right panel) Funnel diagram summarizing the screening subtiers for Tier 1 in the screening funnel. The process is divided into three stages: Tier 1.1. Composition screening; Tier 1.2. Stability/Synthesizability screening; and Tier 1.3. Practical screening.

COMPUTATIONAL COST

leading to high energy densities. Promising operated voltages (\sim 1.7 V vs Zn/Zn²⁺) have also been reported for a wide variety of materials, such as Prussian blue analogues (PBAs) and organic electrodes, albeit with the trade-off of reduced stability over repeated cycles and/or lower volumetric capacities. ¹¹

However, multivalent ions, and Zn²⁺ among them, are known to strongly interact with water and with the host electrode materials, leading to slower diffusion, which, in turn, correlates with reduced reversibility and diminished cyclability. In all divalent intercalating electrode materials, the mobility of the active ion is known to be a primary concern. 9,31 Hence, the design of improved ZIB cathodes will require a deep understanding of Zn mobility. Overall, Zn mobility in ZIBs is known to be primarily influenced by two key characteristics:³² (i) chemical factors, including electronegativity, which directly affects the covalent or ionic nature of bonds between Zn and the surrounding ionic framework; 33,34 and (ii) structural and topological factors, such as the local bonding environment, where stronger bonds may introduce energetic barriers to diffusivity³⁵ and the dimensionality of percolating channels for Zn diffusion. 10 Previous research on Zn-ion battery materials has investigated the influence of these factors, employing them as design rules for the morphological and structural engineering of the diffusion pathways. 11 Zn mobility has also been investigated computationally through screenings of its preferred coordination in both activated and stable sites within different candidate host structures, 36 as well as by systematic studies of Zn intercalation sites and pathways within host materials of diverse chemical compositions. 35-40 However, these studies have typically focused on incorporating or replacing the working ions into known crystallographic sites within the host structures. To date, there have been no extensive screening efforts involving candidate cathode materials that do not contain Zn or other working ions in

their as-synthesized state. In contrast, experimental examples of such "empty-host" Zn cathodes are birnessite-MnO₂, ⁴¹ for which traces of elemental Zn are confirmed by energy-dispersive X-ray (EDX), and V₂O₅ polymorphs, which have been investigated in the preinserted M_xV₂O₅ form (where M = alkali metal, and $1.1 \le x \le 1.2$). ⁴² Hence, screening efforts should include empty intercalation hosts, which often outperform structures containing the migrating ion, ^{9,40} as they often present the active ion in a deep electrostatic potential well, which in turn results in poorer mobility.

In this work, we build upon previous works on Mg⁹ and Ca³¹ cathodes, employing existing automated computational infrastructure ^{9,43} to expand our understanding of the chemical space for divalent-ion batteries and to identify candidate high-voltage multivalent cathodes for ZIBs. We first use screening criteria to select the most promising intercalation hosts, followed by high-throughput density functional theory (DFT) calculations to explore the intercalation of Zn²⁺. We maintain the possibility for aqueous applications by integrating a well-established screening criterion to evaluate candidate stability against passivation and corrosion in aqueous environments, while also predicting the composition of the resulting passivation products. ^{44,45} We then investigate ion mobility in the most promising Zn cathodes, highlighting the factors that influence Zn diffusivity.

■ METHODS: CATHODE DISCOVERY PIPELINE

The screening funnel, represented on the left in Figure 1, follows a similar strategy to previous searches ^{9,43} for multivalent cathodes, in which successive tiers of the funnel require increasingly demanding calculations. This approach helps to minimize the use of more resource-intensive methods, applying them only to a smaller set of promising candidates.

Tier 1: Property Screening. In the initial Tier 1 screening, we select materials with desirable properties from the 2023.11.1 version of the Materials Project (MP) database, 46,47 which contains 163,109

materials. The property screening is then divided into three subtiers, represented on the right in Figure 1.

Further details on the screening tiers, including specifics and metrics on the applied filters, are provided in Section S1.1 of the Supporting Information (SI) of this manuscript. In this tier, candidates were assessed as follows. (1.1) Composition Screening: Exclusion of chemically a priori undesirable compositions, which includes precious metals, radioactive, toxic, and redox-inactive elements. To focus our effort on empty-host materials, in this tier we also exclude Zn or other known working ions to simplify the evaluation of ion mobility and diffusivity. This screening narrowed the pool of potential candidates from 163,109 to 22,769 structures; (1.2) Stability/Synthesizability Screening: Exclusion of materials that may be too unstable to be synthesized or survive in the specific electrochemical working conditions for high-voltage ZIBs. This filter includes the evaluation of known descriptors for thermodynamic stability, such as the energy above the hull (the distance of a phase from the convex energy hull of its most stable phases)^{48,49} as well as a screening for reasonable thermodynamical stability against dissolution, passivation and/or corrosion in the event of aqueous applications. In total, this filter reduced the number of candidates from 22,769 to 6,980 viable materials. (1.3) Practical Screening: Selection of cost-effective and high-performance materials. This screening tier excluded elements with large cost-to-capacity ratios as well as structural frameworks presenting similar crystal structure types and different transition metal (TM) ratios (e.g., NASICON structures (TM)₂(PO₄)₃ with different TM combinations). This final screening tier reduced the optimal candidates from 6980 to 4297 structures, belonging to 1181 distinct crystal structure types. Overall, this process narrowed the initial 163,109 structures to 1181 candidates.

Tier 2: Ion Insertion. To identify potential intercalation sites for Zn²⁺, an insertion algorithm⁵⁰ based on DFT-calculated electronic charge densities was employed to insert Zn2+ ions in empty-host structures. The algorithm was repeated for multiple Zn insertions until (i) the transition metal element in the resulting intercalated structure reaches the lowest available oxidation state; or (ii) a structural mismatch between the intercalated and empty-host structures occurs, indicating nontopotactic intercalation; 43 or (iii) the new structure is rendered too unstable; or (iv) the volume change is larger than 20%. This tier required the calculation of several DFTcalculated properties for the intercalated structures, including stability, average intercalation voltage, energy density, and optimized inserted structure, making it computationally expensive and hence impractical for large material databases. For this reason, we restricted the ion insertion calculations to candidate structures containing common high-voltage TMs (Mn, Co, Cr, and Ni). Out of the 1181 candidates, the ion insertion calculations were successfully completed for 313 of

Additional Screening and Prototype Matching. The topperforming intercalated materials from the insertion electrode calculations were further screened based the properties calculated in Tier 2, selecting high-performance materials (presenting high average intercalation voltages, gravimetric capacities, and energy densities >300 Wh/kg). The materials, as a function of state of charge, were then filtered for stability against conversion reactions⁵¹ using data from the Materials Project PhaseDagram⁵² and PourbaixDagram⁵³ modules in pymatgen.⁵⁴ A more detailed description of the filtering criteria is provided in the SI. These conditions, not present in previous cathode pipelines, 9,31 ensured that candidate materials were thermodynamically stable and exhibited reasonable protection against dissolution in aqueous media. 10,44 This screening reduced the 313 candidates obtained in Tier 1 to the 37 bestperforming materials. For the last tier of calculations, priority was given to candidates whose structural frameworks closely matched known synthesized materials among the 37 best performers. The framework assessment was conducted by matching structures to those in the 5.3.0 version of the Inorganic Crystal Structure Database (ICSD) via pymatgen through both exact and "looser" structure matches, accounting for structural disorder and doping. In the subset structure match, we permitted matches between candidate and ICSD

materials upon substitution of candidate TM sites with other isovalent TMs, and/or substitution of chalcogen and halide sites with other members of their respective groups. The structure matching between the structures was performed using the default tolerance factors. While the exact polymorphs and compositions of the proposed candidates do not correspond to known ICSD entries, we note that several of the best-performing materials exhibit structural similarity to experimentally synthesized compounds. In this final screening tier, out of the 37 top candidates, 12 met the "subset structure match" criteria, indicating structural similarity to experimentally synthesized materials. These 12 candidates were then subjected to mobility calculations, which are detailed in the following section.

Tier 3: Ion Mobility. In the third tier of the screening funnel, the working ion sites of the top 12 performers were used to construct a MigrationGraph, ⁵⁵ mapping the interconnected network of metastable ion sites through a series of "hops". ⁴³ This step identifies symmetrically equivalent sites and hops, generates potential migration pathways, and collects them into a periodic MigrationGraph document. ⁵⁶ Compounds without periodically repeatable Zn migration were discarded, limiting this computationally expensive step to only the candidates that display feasible migration.

As an approximation of Zn²⁺ mobility, we used ApproxNEB⁵⁷ to evaluate the energy profile of the migration pathways. ApproxNEB, as implemented in the atomate 58 and atomate 259 packages, offers a robust and efficient alternative to nudged elastic band (NEB)⁶⁰ by decoupling images along the reaction coordinate and replacing the NEB spring forces with constrained relaxation of the ionic coordinates. In this work, all ApproxNEB calculations were conducted using a structure within the deintercalated/dilute limit with only one Zn ion in the simulation supercell. To accurately represent the dilute limit and avoid self-interaction effects between Zn ions in neighboring periodic cells, the intercalated structures were generated using pymatgen⁵⁴ to ensure that periodic Zn images are at least 7 Å apart. The structures were then relaxed using DFT with the working ion and its antipodal site fixed, yielding the migration energies. In particular, the energy barriers associated with the hops between sites were calculated and mapped onto their respective migration graphs, calculating the shortest percolating pathways through Dijkstra's algorithm. ApproxNEB is known to overestimate migration energy $(E_{\rm m})$ values compared to NEB, as it is not guaranteed to yield images on the minimum energy path of the potential energy surface, unlike NEB. 9,31,43,57 For this reason, ApproxNEB energy barriers provide an upper limit of the barrier in our screening process. While original studies have reported deviations on the order of ~20 meV for barriers in the 200-1000 meV range,⁵⁷ more recent work on Mg and Ca systems has shown that ApproxNEB-predicted barriers typically lie within 150-170 meV of full NEB results. 9,31 In light of those benchmarks, assuming nanosized materials, we adopt a migration energy threshold of ~ 1 eV.⁴⁰

In this screening protocol, 9 of the ApproxNEB workflows obtained for the 12 top candidates identified via the ICSD subset match successfully converged, revealing possible pathways for Zn²⁺ migration. In particular, four materials exhibited a percolation barrier below the 1 eV threshold for at least one migration pathway and have thus been identified as promising in terms of ion mobility and synthetic viability. The details and energetic landscapes of the calculated pathways are the subject of the following section and of Section S3 of the SI of this work. Once promising materials are identified through ApproxNEB calculations, further in-depth diffusion analyses—such as climbing-image (CI)-NEB calculations⁶¹ and ab initio molecular dynamics (AIMD)—can be employed to gain a more comprehensive understanding of the energetics and morphology of the migration network.

■ RESULTS AND DISCUSSION

Screening Results. Here, we expand on the results obtained from the screening pipeline, highlighting the key findings obtained from the analysis of the most promising candidates.

Average Voltage vs Capacity

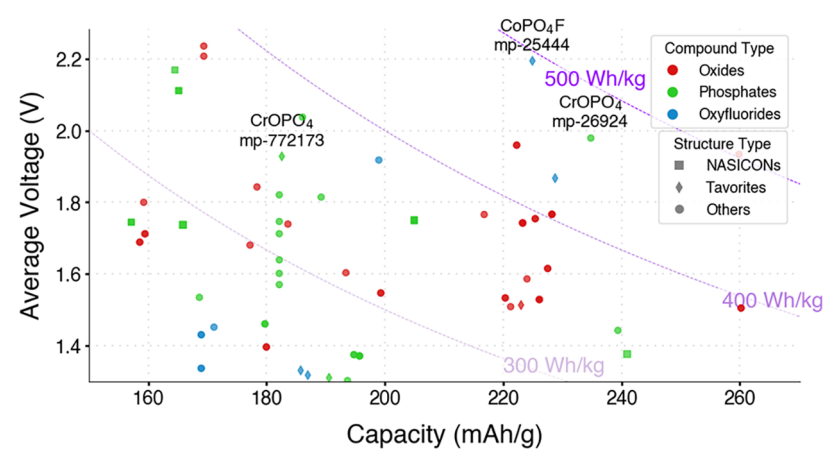


Figure 2. Distribution of best-performing candidate materials resulting from Tier 2 by average voltage and theoretical capacity.

Voltage vs Redox Pairs

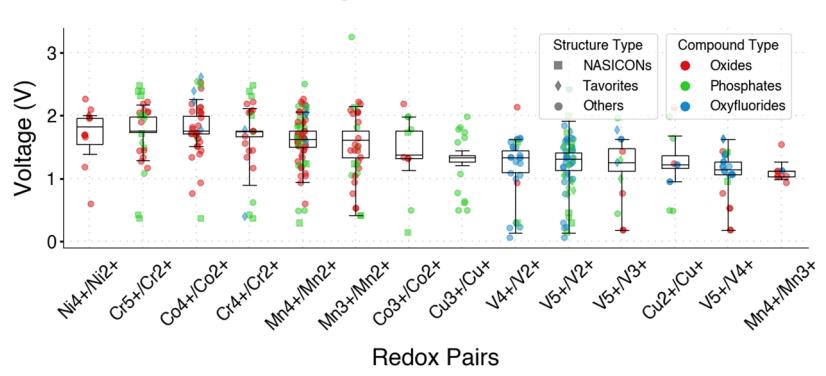


Figure 3. Voltage distribution (max and min voltages) of the best candidates as a function of the most common redox pairs in the host structures. The statistical analysis was conducted on the average voltages of the candidates, which are plotted in decreasing order of median average voltage.

Of the candidates identified in Tier 1, 88.2% are filtered out by the Tier 2 criteria: 21.7% due to low average theoretical intercalation voltages, 62.6% due to stability requirements, and 42.5% with below-threshold gravimetric capacities or energy densities.

Notably, this refinement stage excludes well-known host frameworks such as MnO₂ and V₂O₅ polymorphs, which, despite favorable chemistry, do not simultaneously meet all of the additional screening criteria in Tier 2. In particular, their predicted insertion voltages fall below the 1.3 V threshold. These findings are consistent with previous studies: for birnessite-MnO₂, the average intercalation potential was calculated as 1.12 V (1.15 in ref 41), while for V₂O₅ polymorphs, average voltages were calculated around 0.72 V and experimentally measured as 0.7 V in M_xV₂O₅ phases (where M = alkali metal, and 1.1 \leq x \leq 1.2).⁴² It is important to note that if lower-voltage applications are of interest, then the screening criteria should be revised to reflect those requirements.

Figures 2 and 3, summarize the outputs of Tier 2, representing the overall performance (Figure 2) and voltage windows (Figure 3) of the top candidates (gravimetric energy density >300 Wh/kg) resulting from the ion insertion step, including the four best candidates obtained at the end of the screening procedure (Figure 2). However, we find that the average intercalation potentials of the top candidates exceed

the oxygen evolution reaction (OER) potential, which occurs at approximately 0.9-0.94~V vs standard hydrogen electrode (SHE) ($\sim 0.1~V$ vs Zn/Zn^{2+}) in the pH range relevant to aqueous applications (pH = 5-5.5). This suggests that these materials may only be amenable for aqueous applications with specialized electrolytes, e.g., water-in-salt WISE electrolytes. 62,63

Based on the screening results of Figure 3, and in accordance with known chemical trends, 64,65 oxyfluorides and phosphates exhibit higher voltages compared to oxides. In particular, the candidates with the highest voltages were predominantly polyanion compounds, specifically (fluoro)phosphates. This trend conforms with the well-established strong inductive effect of polyanion groups and is commonly observed in both Li-ion^{64,65} and Na-ion⁶⁶ batteries, where (fluoro)phosphate cathode materials typically exhibit very high voltages. Similar considerations can be made in terms of the redox center. Figure 3 demonstrates that cations such as Ni⁴⁺, Co⁴⁺ and Cr⁵⁺ exhibit higher voltage distributions, which correlates with heavier redox-active cations within the same period or those with higher oxidation states. 67,68 A more detailed description of the effect of the polyanions and the redox centers on the potential of the host materials is provided in the Structural and Chemical Effects section. The results demonstrate the effectiveness of our screening protocol, as the targeted approach significantly narrows the candidate pool, restricting

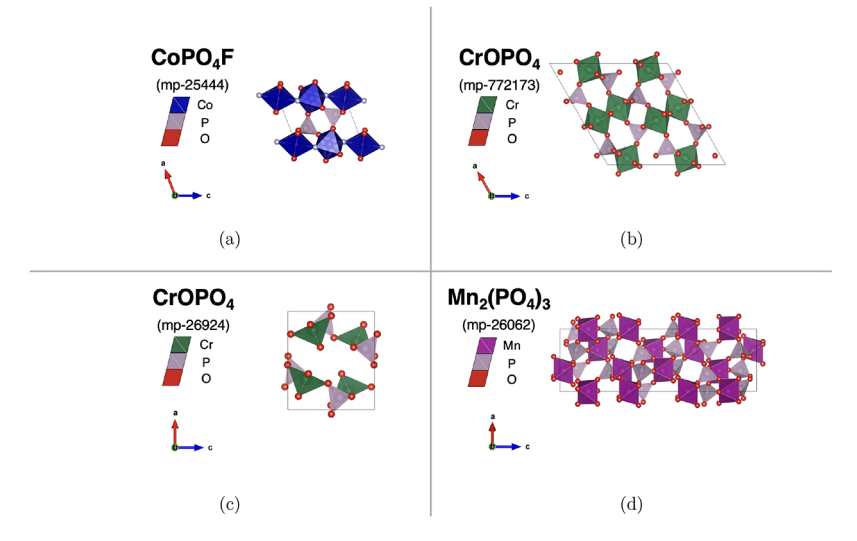


Figure 4. Unit cell crystal structures of the best-performing candidates obtained from the screening pipeline: (4a) triclinic tavorite CoPO₄F (mp-25444), (4b) monoclinic tavorite CrOPO₄ (mp-772173), (4c) orthorhombic Cr phosphate CrOPO₄ (mp-26294), and (4d) trigonal NASICON Mn₂(PO₄)₃ (mp-26062).

Table 1. Summary of Electrode Properties for the Four Best-Performing Zn Cathodes

formula mp-id	symmetry	Pourbaix $\Delta G_{ ext{max}}$ (eV/atom)	intercalation voltage (V)	$\frac{\Delta V}{(\%)}$	gravimetric capacity (mAh/g)	gravimetric energy density (Wh/kg)	charge stability (eV/atom)	ApproxNEB barrier (meV)	prototype
CoPO ₄ F (mp-25444)	P1 (triclinic)	0.30	2.19	6	224.93	493.60	0.10	772 (1D) (2D with 1.2)	SbOPO ₄ (mp-9750) (icsd- 201743)
CrOPO ₄ (mp- 772173)	P2 ₁ /c (monoclinic)	0.34	1.93	6	182.57	352.01	0.10	958 (1D)	NbOPO ₄ (mp-542453) (icsd-93766, icsd-40870, icsd-93767, icsd-252566)
CrOPO ₄ (mp-26924)	Pnma (orthorhombic)	0.30	1.98	4	234.71	464.82	0.05	774 + 951 (1D)	VOPO ₄ (mp-25265) (icsd-291605, icsd-9413)
$\frac{\text{Mn}_2(\text{PO}_4)_3}{(\text{mp-26062})}$	$R\overline{3}$ (trigonal)	0.45	1.77	20	240.02	424.23	0.06	894 (3D)	Nb ₂ (PO ₄) ₃ (mp-17242) (icsd-65658)

computationally expensive ion diffusion calculations to only the most promising host materials. Thirty seven candidates—around 12% of the 313 electrode candidates that underwent insertion calculations—met the additional screening criteria in the second phase of Tier 2. This selection was further refined by the prototype matching, yielding 12 final candidates (about 4% of the initial pool).

As is discussed in the Structural and Chemical Effects section, various polymorphs (e.g., CoPO₄F, ^{69,70} MnP₂O₇ ⁴³) and/or compositions of some of these 12 candidates have been investigated as intercalation electrodes in previous work on known cathode prototypes for Zn and other working ions (e.g., the study of Na intercalation/deintercalation mechanism in doped equivalents of Mn₂(PO₄)₃ such as MnV(PO₄)₃⁷¹ and of $Mn_3V_2(PO_4)_3$ in ZIBs):⁷² however, the specific compositions of these materials have to our knowledge not been considered for Zn-ion intercalation. Furthermore, our approach also revealed several promising candidates that have not yet been explored in literature (e.g., Mn₂(PO₄)₃), highlighting the potential of the employed pipeline for the discovery of promising novel materials. Following the final ApproxNEB step in the pipeline, 4 out of 12 candidates were selected, as they demonstrated the most favorable migration pathways and energetics. The four best-performing candidates resulting from the overall cathode discovery pipeline are represented in Figure

4. Their IDs, calculated properties, and ICSD prototypes are represented in Table 1.

We proceed to analyze the results of the calculations performed in Tier 2 and Tier 3, identifying the topology of the ion insertion sites and of the corresponding percolation pathways.

ApproxNEB Results. As discussed in the Tier 3: Ion Mobility section, efficient kinetics are crucial for utilizing Zn as a working ion in prospective battery materials. Therefore, we employed ApproxNEB calculations to evaluate the Zn migration pathways for the top candidates identified in Tier 3. We define a percolating pathway as the trajectory from a Zn site within a unit cell to a periodic site in an adjacent unit cell. Each pathway comprises symmetrically distinct hops between intercalation sites, or endpoints. The endpoints are labeled as A, B, etc., in order of increasing destabilization (i.e., insertion energy), with numerical subscripts distinguishing different endpoints of the same energy. Periodic images are indicated using a superscript prime symbol '. We emphasize that the pathways are analyzed in the dilute lattice limit, as these materials are synthesized in their charged state. While low barriers in this limit are a necessary criterion, they are not sufficient, as cation-cation interactions can hinder mobility and reduce rate capability in the partially discharged state.

Overall, four of the candidates presented a barrier below the 1 eV threshold for at least one percolation pathway. The

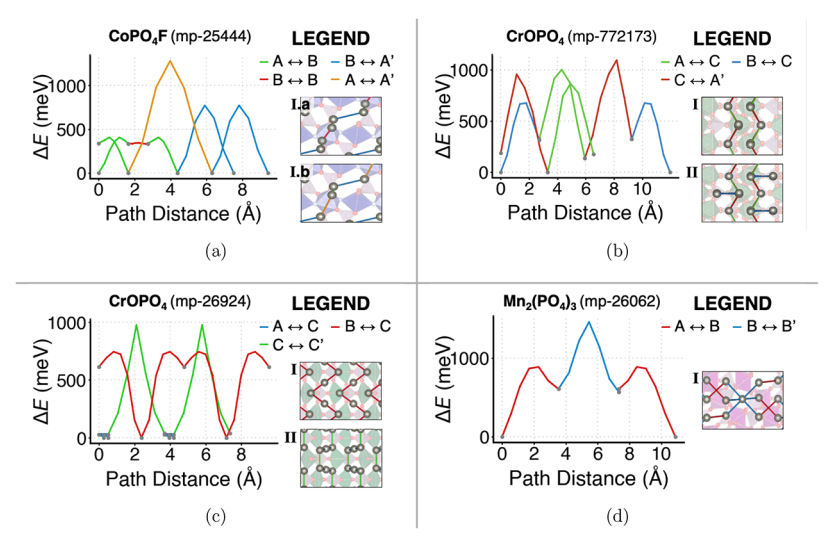


Figure 5. Energy landscape plots for Zn²⁺ migration along the percolating pathway with the lowest kinetic barriers in the four candidate materials. Each hop in the energy profile (left) is mapped with the same color in the pathway (right) and labeled through its endpoints, which are defined as symmetrically unique positions through the notation in this section. (a) Triclinic tavorite CoPO₄F (mp-25444), exhibiting energetic barriers of 772 and 1283 meV over total path distances of 7.51 and 9.43 Å (both Pathway I, left and right), respectively. (5b) Monoclinic tavorite CrOPO₄ (mp-772173), both with an energetic barrier of 958 meV, across total path distances of respectively 6.55 Å (Pathway I, on the left) and 11.95 Å (Pathway II, on the right). (5c) Orthorhombic Cr phosphate CrOPO₄ (mp-26924), showing energetic barriers of 774 and 951 eV along a total path distance of 9.55 Å (Pathway I, on the left) and 7.39 Å (Pathway II, on the right), respectively. (d) Trigonal NASICON Mn₂(PO₄)₃ (mp-26062), with an energetic barrier of 894 meV over a total path distance of 10.88 Å.

ApproxNEB results for these materials show the following energy barriers for Zn migration: 772 meV for $CoPO_4F$ (mp-25444), 958 meV for $CrOPO_4$ (mp-772173), 951 meV for $CrOPO_4$ (mp-26924), and 894 meV for $Mn_2(PO_4)_3$ (mp-26062). In Figure 5, we present the calculated energy profiles for the most kinetically favorable pathways for long-range Zn migration in the four best candidates. A detailed representation of the energy profiles of the hops involved in each pathway is provided in Figures S7–S17 in Section S3. The screening results indicate that $CoPO_4F$ (mp-25444) shows potential as a high-energy-density ZIB cathode. However, nanosizing and testing under repeated cycling conditions are needed as the limited Zn^{2+} mobility could lead to reduced stability and poor rate capability over time. ⁷³

CoPO₄F (mp-25444). As shown in Table 1, CoPO₄F (mp-25444) exhibits an average theoretical Zn intercalation voltage of 2.19 V vs Zn/Zn²⁺, and a volume change of 6%. It should be noted that ZnCoPO₄F is close to the limit of our stability criteria, with the fully intercalated state (ZnCoPO₄F) exhibiting an energy above the hull of 100 meV/atom and its charged phase at 121 meV/atom. According to the Materials Project phase diagram, 45,46 ZnCoPO₄F is predicted to decompose into Zn₃(PO₄)₂, Co₃(PO₄)₂, and CoF₂, indicating that full theoretical 224.93 mAh/g gravimetric capacity and 493.60 Wh/kg energy density may not be achievable. For aqueous electrolyte applications, CoPO₄F is 300 meV/atom unstable against P(OH)₂⁻, F⁻, and Co(OH)₂, which means that a Co(OH)₂ surface passivation layer may form in aqueous applications.

CoPO₄F crystallizes in the low-symmetry triclinic $P\overline{1}$ space group, with calculated lattice parameters of a=5.27 Å, b=5.30 Å, c=7.39 Å and relative angles of $\alpha=108.57^{\circ}$, $\beta=107.81^{\circ}$, $\gamma=95.60^{\circ}$. This candidate belongs to the tavorite family: its structure features two inequivalent Co sites, both forming CoO_4F_2 octahedra that share corners with two other CoO_4F_2 octahedra and four equivalent PO_4 tetrahedra.

In this candidate, Zn can be inserted into one of two symmetrically unique positions, labeled A and B. The B site corresponds to the least stable Zn configuration, as it is located closer to a cation (the Co atom in a CoO_4F_4 octahedron). ApproxNEB calculations confirm a main one-dimensional (1D) pathway characterized by three symmetrically unique hops (Figure 5a): a 407 meV hop between adjacent A and B sites (A₁ and B₁), a 13 meV hop between two B sites (B₁ and B₂), another 407 meV hop between adjacent A and B sites (this time in the reverse direction, i.e., between B and an adjacent A site), and a 772 meV hop between two A sites (A₂ and A_1), terminating in a different unit cell. This pathway, named Pathway I.a, thus follows the sequence: $A_1 \rightarrow B_1 \rightarrow B_2$ \rightarrow A'₂ and \rightarrow A'₁. An alternative sequence of hops for Pathway I.a could involve replacing the two intermediate hops with a 448 meV hop between the A₂ site and the nonadjacent B₂ site, leading to an overall $A_1 \rightarrow B_2 \rightarrow A_2' \rightarrow A_1'$ with the same dimensionality that terminates in a periodic A₁ position in a separate unit cell. This alternative sequence Pathway I.b, though highly hindered (with a 1283 meV hop between the A₁ and A2 sites), could extend the system's network to two dimensions. A two-dimensional (2D) pathway would be desirable in order to reduce the probability that defects and impurities block Zn migration.

CrOPO₄ (mp-26924, mp-772173). In our cathode screening pipeline, two polymorphs of CrOPO₄ were identified as potential candidates for Zn-ion cathodes: a monoclinic polymorph, mp-772173, and an orthorhombic polymorph, mp-26924. Table 1 highlights the calculated electrochemical properties of the two polymorphs. The first polymorph, mp-772173, displays a higher theoretical intercalation voltage (1.98 V vs Zn/Zn²⁺), greater energy density (464.82 Wh/kg), and smaller volume change (4%) compared to mp-26924, which has an intercalation voltage of 1.93 V vs Zn/Zn²⁺, an energy density of 352.01 Wh/kg, and a 6% volume change. The monoclinic polymorph belongs to the $P2_1/c$ space group with

lattice parameters of a = 12.68 Å, b = 5.04 Å, c = 12.80 Å and relative angles of 108.57° , $\alpha = \gamma = 90.00^{\circ}$, $\beta = 119.81^{\circ}$. The structure of this polymorph is less stable, with a charge state energy above the hull of 100 meV/atom against CrO2, CrPO4, ZnCr₂O₄, and Zn₃(PO₄)₂. In aqueous applications, the discharged phase Zn_{1.5}CrOPO₄ displays a 340 meV/atom decomposition energy into Zn^{2+} , $P(OH)_2$, and $Cr(OH)_4$, indicating that a phosphorus hydroxide-rich surface passivation layer may form. Similarly to the first candidate (CoPO₄F, mp-25444), this candidate structurally belongs to the tavorite family. As such, it features two inequivalent Cr sites forming CrO₆ octahedra, which share corners with two equivalent CrO₆ octahedra and four equivalent PO₄ tetrahedra. Zn intercalation in this polymorph of CrOPO₄ can occur in three symmetrically unique sites, labeled A, B, and C in order of decreasing stability. ApproxNEB calculations for this material confirm a one-dimensional diffusion pathway (Pathway I), where Zn ions hop between adjacent C and A sites, alternating between consecutive, symmetrically unique 866 and 958 meV hops. Unfortunately, in this specific polymorph, the Approx-NEB results did not highlight the presence of alternative Zn migration pathways that could expand the dimensionality of the diffusion framework. However, as shown in Figure 5b this pathway can, in principle, offshoot into a 676 meV hop between adjacent B and C sites, providing access to otherwise inaccessible metastable sites and forming an expanded 1D diffusion pathway (Pathway II) that is a superset of Pathway I, increasing the theoretical capacity of the material while maintaining the overall 1D dimensionality of the migration pathway. This result is consistent with the literature: as further expanded in the Evaluating Material Design Rules section, tavorite-based materials have been associated with lowerdimensional migration pathways due to the high-overlap motifs present between their polyhedra.

On the other hand, the intercalated structure of this second polymorph, mp-26924 (also Zn_{1.5}CrOPO₄), exhibits an energy above the hull = 47 and 300 meV/atom in aqueous media, yielding $Cr(OH)_4^-$ and $P(OH)_2^-$ as decomposition products. It crystallizes in an orthorhombic symmetry (*Pnma* space group), with lattice parameters of a = 6.09 Å, b = 7.16 Å, c = 8.13 Å and relative angles of $\alpha = \beta = \gamma = 90.00^{\circ}$. In this structure, Cr5+ ions form CrO5 trigonal bipyramids, cornersharing with four equivalent PO₄ tetrahedra. ApproxNEB calculations for this structure in the dilute limit confirm a onedimensional pathway (Pathway I) defined by four symmetrically equivalent 744 meV hops, where Zn ions migrate between B and C sites, creating a "tunnel" hop between noninterconnecting CrO₅ polyhedra. There is, however, an alternative 1D pathway (Pathway II) that enables another channel for Zn-ion mobility in the structure. This pathway involves two symmetrically inequivalent hops: a 34 meV hop between A and C sites, and a 951 meV hop between adjacent C sites. This alternative pathway maintains the same overall "intertunnel" direction for Zn migration as the primary 744 meV pathway (Figure 5c).

Even though the mp-26924 polymorph of CrOPO₄ exhibits a migration pathway with a barrier of 774 meV (Pathway I), both polymorphs display similar ApproxNEB migration barriers (951 meV for mp-26924, and 958 meV for mp-772173) for the other migration pathways (respectively Pathway II for mp-26924 and Pathway I/II for mp-772173), and are classified as 1D diffusers. This result may pose challenges for the performance of the material unless

nanosized.⁷⁴ However, the presence of multiple migration pathways in mp-26924 suggests that symmetry breaking within structures with high-overlap motifs, such as tavorites, could introduce alternative, potentially lower-energy migration pathways.

 $Mn_2(PO_4)_3$ (mp-26062). Table 1 displays the theoretical properties calculated for NASICON $Mn_2(PO_4)_3$ (mp-26062). The discharged structure $Zn_{0.5}Mn_2(PO_4)_3$ exhibits an average intercalation voltage of 1.77 V vs Zn/Zn^{2+} , a volume change of 20%, and an aqueous instability = 450 meV/atom against $P(OH)_2^-$, Zn^{2+} , and MnO_4^- . Its intercalated phase exhibits an energy above the hull 60 meV/atom and a high theoretical gravimetric capacity of 240.02 mAh/g and energy density of 424.23 Wh/kg.

 $Mn_2(PO_4)_3$ belongs to the trigonal $R\overline{3}$ space group. Consistent with its trigonal symmetry, its calculated lattice parameters a = b = 8.16 Å, c = 22.25 Å, and relative angles of α $= \beta = 90.00^{\circ}$, $\gamma = 120.00^{\circ}$. $Mn_2(PO_4)_3$ adopts a threedimensional (3D) structural framework, presenting two inequivalent Mn sites forming MnO₆ octahedra, which share oxygen corners with six equivalent PO₄ tetrahedra. In this structure, Zn can be intercalated in one of two nonsymmetrically equivalent Zn sites, labeled A and B, with the former being lower in energy due to its location in a low-energy cavity (1a Wyckoff position). The ApproxNEB calculations for this material reveal multiple migration pathways, each presenting three hops: two symmetrically equivalent 886 meV hops connecting A and B sites and one symmetrically unique 894 meV hop between adjacent B sites. Multiple pathways are identified in the host structure, resulting in a 3D migration network (Figure 5d). This result is consistent with previous findings for LISICON and NASICON-type frameworks, which demonstrate remarkable Li+ diffusivity and reversibility in repeated cycling due to the topological patterns present in this family of materials, providing high-volume cavities for ion intercalation and migration.75

EVALUATING MATERIAL DESIGN RULES

In the Introduction section, we highlighted the importance of identifying key features that influence the mobility of the working ion, which are essential for designing performant positive electrode materials. These factors may include structural aspects—such as polyhedral distortions, ^{79,80} the density of the host framework (e.g., the volume per anion/cation ratio), and low-overlap motifs that facilitate ion migration, ³¹ as well as more chemical/environmental factors, like the coordination environment and stability of mobile ions, ^{40,82,83} and electrostatic interactions of the host framework with the working ion. The following section will highlight the descriptors that have been identified as potential material design principles in the most promising candidate materials, evaluating their impact on Zn-ion diffusion and the overall performance of candidate cathode materials in ZIBs.

Structural and Chemical Effects. As detailed in the Screening Results section, the potential of the screening endeavor in identifying the most promising candidates is confirmed by their similarity to previously investigated structures (e.g., polymorphs) and ICSD prototypes, many of which are recognized as effective materials for intercalation-based energy storage. In response to the focus on high-voltage, high-energy applications, it is not surprising that all four candidates identified through this screening are polyanion compounds, specifically (fluoro)phosphates. As discussed in

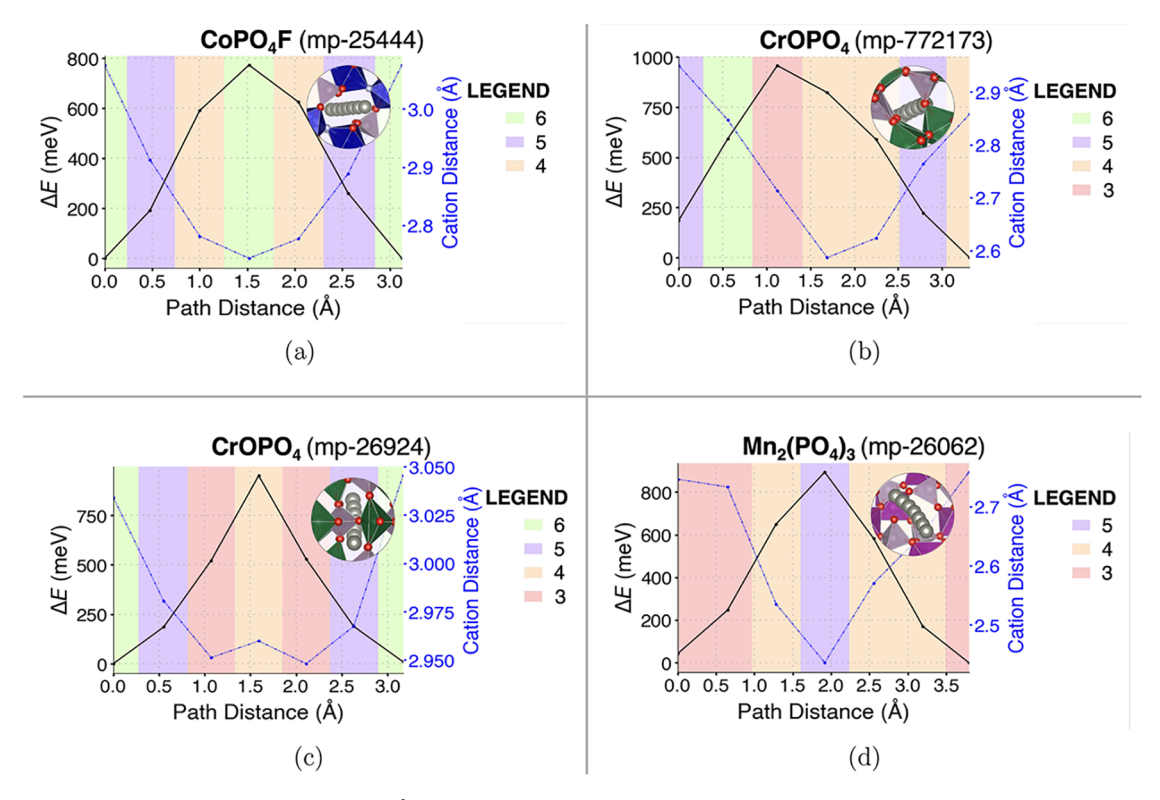


Figure 6. Evolving environment and associated Zn^{2+} migration energy as a function of the pathway coordinate in the four best-performing candidates: (a) $CoPO_4F$, (b, c) the two polymorphs of $CrOPO_4$, and (6d) $Mn_2(PO_4)_3$. Graph of the ApproxNEB energy barrier in the rate limiting step of the migration path (black line with circles), as a function of (i) Zn^{2+} coordination (colored graph area), (ii) Zn^{2+} distance from nearest cation in the host framework (blue dotted line with circles).

the Screening Results section, this trend arises from the strong inductive effect of polyanion groups, where the robust P–O covalency stabilizes the reduced state and enhances the material's redox potential. The presence of fluorine, with its high electronegativity, further amplifies this effect, leading to even higher operating voltages. This trend has been previously observed in both Li-ion^{64,65} and Na-ion⁶⁶ batteries, where (fluoro)phosphates cathode materials typically exhibit high voltages.

A similar trend is observed for the redox centers: the bestperforming candidates present Co4+, Cr5+, and Mn4+/Mn5+ as redox centers in their charged state. These ions align with the expected trends for high-voltage cathodes: ^{67,68} Co⁴⁺, Cr⁵⁺, and Mn⁴⁺/Mn⁵⁺ are all "late" period IV transition metals at high oxidation states, which exhibit small ionic radius, high ionization energies, and, as a consequence, high redox potential. Moreover, the top four candidate materials belong to well-established structural families, such as NASICONs and tavorites. ⁷⁶ For instance, CoPO₄F (mp-25444) and CrOPO₄ (mp-772173) both structurally belong to the tavorite family (general formula $M(XO_4)Y$, where M = Fe, V, Ti, Mn, Co, \cdots , X = P, S, W, ..., Y = F, O, OH^{76}). Tavorite frameworks are known for their high structural tolerance to intercalation, which results in a higher degree of successful topotactic insertion. The insertion sites connect through open channels, enhancing intercalation kinetics and in some cases, enable multichannel ionic transport and fast ion migration. 50 For these reasons, these materials have been extensively studied for their potential in lithium-ion batteries. While similar compounds (e.g., VPO₄F and FePO₄F, as well as orthorhombic polymorphs of CoPO₄F) have shown promise as cathodes in monovalent ion batteries, ^{69,87–93} the triclinic polymorphs of

CoPO₄F and CrOPO₄ remain experimentally unexplored. However, their frameworks match ICSD entries such as SbOPO₄ (mp-9750), 94 high-temperature polymorphs of NbOPO₄, specifically β -NbOPO₄ (mp-542453), β -97 and with VOPO₄, which have recently attracted interest as cathode materials for monovalent 55,98,99 and divalent 100,101 ion batteries. Unlike its monoclinic counterpart, the orthorhombic CrOPO₄ polymorph (mp-26924) does not strictly belong to the tavorite family as this form features a more distorted phosphate framework. However, the structure also aligns with the symmetry group of β -VOPO₄ (mp-25265), 102,103 a known framework for 3D ion migration 87,104 and versatile intercalation, 55,98,99 making it reasonable to anticipate a similar behavior from its $CrOPO_4$ polymorph. Notably, ϵ and δ -VOPO₄ were recently identified computationally as viable Mgion cathodes, showing computed NEB barriers of 687 and 588 meV, respectively. 31,100 Experimental studies on the ϵ polymorph demonstrated intercalation supporting energy densities exceeding 200 Wh/kg for small particle sizes (100 nm).5

Lastly, the electrochemical performance of NASICON materials (general formula $M_2(XO_4)_3$, where $M=Fe, V, Ti, Mn, Co, \cdots X=P, S, W, \cdots^{76}$) has also been the object of several previous investigations, highlighting the influence of structural and compositional descriptors—such as polyhedral distortions and disproportionation reactions at the redox-active sites—on the resulting performance and electrical conductivity of these materials and design guidelines various synthetic strategies 105,106 and design guidelines 4,107 to optimize the overall performance of these materials. While specific diffusion pathways for $Mn_2(PO_4)_3$ have yet to be reported, NASICONtype phosphates have been widely investigated as cathode

ı

materials for both Li and Na-ion batteries. 75,76 Mn₂(PO₄)₃, in particular, shows an ICSD subset match to Nb₂(PO₄)₃ (mp-17242), 108 a known anode material in Li- and Na-ion batteries 109 characterized by diagonal diffusion paths, suggesting that a similar diffusion behavior might be expected for Mn₂(PO₄)₃.

A more detailed description of the computational and experimental research on these materials, including similar compositions, polymorphs, and ICSD framework matches, is provided in Section S2 of the SI of this work. Overall, the structural parallels displayed by the candidate materials to studied cathode frameworks show that known structural motifs can be applied for the prediction and design of new intercalation hosts, emphasizing the role of structure as a transferable descriptor for ion mobility.

Evolving Environment. The changing crystalline environment surrounding the working ion throughout a migration event, known as the evolving environment,9 is another descriptor affecting the mobility of the working ion. This descriptor originated from work by Rong et al.,40 which illustrated a correlation between migration barriers and ion topology in host frameworks. In the paper, the authors suggested that higher barriers often occur in environments in which the preferred coordination number of the working ion matches its effective coordination in the host. This trend has been confirmed in computational screening studies for Mg²⁺ and Ca^{2+9,31} electrode materials, motivating further exploration into the behavior of Zn2+. Zn2+ is known to exhibit a preferred 4- or 6-fold coordination depending on the anion/ base strengths of the surrounding ions and on the spatial constraints of the evolving environment. 110

In our calculations, we quantified the influence of the evolving environment on the energy landscape of Zn^{2+} migration in candidate materials. In particular, in Figure 6a–6d we show the Zn^{2+} energy landscape of the four best-performing candidates in the most kinetically hindered hops (or bottleneck hops), represented using the VESTA software of the ApproxNEB migration pathways analyzed in the ApproxNEB Results section, as these provide an indications of the factors that affect ion mobility in Zn^{2+} diffusion. The plots are color-coded to depict the varying Zn^{2+} coordination at different positions along the migration hops, as analyzed using the Crystalnn algorithm in pymatgen. S4,112 They also depict the distance between mobile Zn^{2+} and the nearest cation (on average) in the host structure.

In general, poor migration is expected to arise in materials where Zn2+ resides in a strong potential well, leading to restricted mobility. Conversely, improved mobility is expected for topologies where the mobile ion is stabilized by its preferred coordination at the activated site. However, notably, we find that in these materials the strongest influence on the activation barrier is the repulsion between the Zn²⁺ and the closest cation. For instance, in CoPO₄F (mp-25444), the highest-energy point occurs when 6-fold coordinated Zn squeezes through an anion cavity formed by four O atoms and two F atoms in equivalent, non-corner-sharing CoO₄F₂ octahedra. In the two $CrOPO_4$ polymorphs and in $Mn_2(PO_4)_3$, the migration energy bottleneck occurs when Zn migrates through anion cavities formed between redox-active TM polyhedra and PO₄ tetrahedra—respectively three O atoms in adjacent CrO₆ octahedra in CrOPO₄ (mp-772173), resulting in 3-fold coordination, four O atoms in CrO₅ trigonal bipyramids in CrOPO₄ (mp-26924), displaying 4-fold

coordination, and five O atoms in nonadjacent PO₄ tetrahedra in Mn₂(PO₄)₃ (mp-26062), corresponding to 5-fold coordination for Zn. As shown in Figure 6, in the majority of cases, the highest-energy points correspond to the closest distance between Zn and its nearest cation and/or to the lowest Zn coordination in the host. Interestingly, at shorter Zn-cation distances (<2.7 Å), we observe a modulation between coordination and electrostatics. This modulation is evident in the case of CrOPO₄, for which the activation barrier is set for the 3-fold coordinated site, slightly offset from the closest cation-cation distance. The high energy results from a combination of structural constraints, which restrict the available space for Zn diffusion within the host structure, and electrostatic repulsion between Zn and the closest cation. Similar effects are well-known in the layered and rocksalt Liion cathode materials: 40 first shown by Van der Ven and Ceder, 82,113,114 lithium migration follows a divalent mechanism via a tetrahedral activated state, where the migrating Li+ remains in close proximity to a transition metal. This model predicts maximal lithium diffusivity in partially delithiated phases, aligning with experimental observations. Higher Li diffusion was attributed to Li vacancies, which lower the energy of the activated states by decreasing the electrostatic repulsion between the activated lithium ion and its neighboring cations, and was later confirmed for a variety of layered and spinel materials. 85,86,115 While initial descriptor development on monovalent ions such as Li focused on mixed descriptors, e.g., coordination and nearest-cation distance, our prior studies on multivalent systems focused on coordination as the main descriptor. For Mg²⁺, coordination number and local volume along the diffusion path were found to correlate with migration barriers,9 whereas for Ca2+, variations in coordination environment and overlap of nearest-neighbor shells along the migration path were selected as descriptors.³¹ In the case of Zn²⁺, we find that coordination number alone does not adequately capture the energy landscape. Instead, the Zncation distance emerges as the most consistent descriptor, correlating with the softer and more covalent nature of Zn²⁺, which results in different interactions with the host lattice compared to those with harder divalent cations such as Mg²⁺ and Ca²⁺. Additionally, in a similar fashion to Li, we note that at high charge, the repulsive interaction between Zn and the transition metal in the host structure is significantly influenced by the oxidation state of the transition metal, as higher oxidation states will result in higher electrostatic interactions with the migrating ion and, leading to higher activation barriers. 86,113,114,116 Interestingly, while current Li-ion cathodes are synthesized in the discharged state—where repulsive interactions intensify as the transition metal valence state increases, the candidate Zn-ion cathodes, for which the computed barriers correspond to the charged state, are expected to exhibit a decrease in cation repulsion with increased intercalation and with the consequent reduction of the redox-active transition metal centers. Overall, our work underscores the crucial influence of both structural and electrostatic interactions on ion mobility, offering insights into the design of next-generation multivalent battery materials. Indeed, previous studies conducted on Mg²⁺ indicated that the coordination number, while important, might not be an adequate descriptor for the energy profile of the migration pathway, suggesting that the electrostatic landscape of the host material plays a significant role in

defining the energetic landscapes (and penalties) of ionic migration.

CONCLUSIONS

In this study, we employed a high-throughput computational screening pipeline to identify high-performance cathode materials for Zn-ion batteries (ZIBs). Our automated discovery pipeline narrowed down the initial dataset of 163,109 candidate materials from the Materials Project database through increasingly selective and more resource-intensive tiers. The first stage applied property screening based on composition, stability, and synthesizability and practical considerations, focusing on key performance descriptors such as operating voltage windows and gravimetric energy densities. The screening criteria were then integrated with density functional theory (DFT) calculations to evaluate Znion intercalation and diffusion in the materials, further refining the selection through comparison with similar, experimentally synthesized structures from the Inorganic Crystal Structure Database (ICSD).

Focusing on high-voltage cathode applications, the initial dataset was narrowed to four top-performing candidates: CoPO₄F (mp-25444), two polymorphs of CrOPO₄ (mp-772173, mp-26924), and Mn₂(PO₄)₃ (mp-26062). Our analysis of these materials for material design descriptors emphasized a correlation between ion mobility and common structural motifs in the host structures: the high voltages presented by the four best candidates are attributed to the stabilizing effect of phosphates and fluorophosphates on highvoltage redox centers through inductive effect, as well as the presence of "late" period IV transition metals at high oxidation states (Co⁴⁺, Cr⁵⁺, and Mn⁴⁺/Mn⁵⁺). These trends, previously observed in Li- and Na-ion batteries, 64-68 are here extended to ZIBs. Furthermore, the presence of feasible intercalation sites/ pathways and favorable migration barriers (<1 eV) is ascribed to structural features of the host frameworks, which present high tolerance to intercalation, fully connected migration networks and deviations from the classical frameworks that introduce distorted morphologies. We find that the repulsion between Zn and the nearest cation correlates the most strongly with the activation energy barrier, with slight modulation for the local environment. This suggests that the anticipated migration barriers may be ameliorated at partial discharge.

We note that removing materials with multiple movable ions (e.g., Li⁺, Na⁺, Mg²⁺, Zn²⁺, etc.) in the pipeline also removes the possibility of designing for coordinated motion. Future studies may explore alternative screening criteria, including frameworks containing working ions and/or that have demonstrated high performance with other multivalent ions. However, our results emphasize the effectiveness of a structure-based approach for identifying candidate materials, reinforcing the role of framework topology and connectivity in optimizing ion migration through the host structures.

Future investigations on prospective candidate materials should further investigate Zn-ion mobility and kinetics in the identified candidates through more accurate computational investigations such as climbing-image nudged elastic band (CI-NEB) calculations and ab initio molecular dynamics (AIMD). Experimental validations (synthesis, electrochemical characterization) will also be critical to confirm feasibility, with a particular focus on their stability under prolonged cycling.

Overall, this study refined the preexistent discovery pipeline for cathode materials by linking their performance and ion diffusivity to structural and chemical design principles. By expanding the pipeline to ZIBs, this study has further extended the chemical search space for divalent-ion battery materials, driving the development of safer, cost-effective, and sustainable energy storage technologies.

ASSOCIATED CONTENT

Data Availability Statement

All data presented in this work are available freely and without access restrictions on the MPContribs platform https://next-gen.materialsproject.org/contribs/projects/zn_cathodes_2025. Larger data objects, such as the results of ion intercalation and densities of states, are located separately (again without any access restrictions) on the MPContribs OpenData bucket: http://materialsproject-contribs.s3. amazonaws.com/index.html#zn_cathodes_2025/.

Supporting Information

The Supporting Information is available free of charge at https://pubs.acs.org/doi/10.1021/acs.chemmater.5c00916.

Screening criteria employed in the different tiers; literature review on best candidates (for most common working ions): polymorphs, different compositions, ICSD matches; summary of migration hops and pathways; methodology/computational details employed in the calculations (PDF)

AUTHOR INFORMATION

Corresponding Author

Kristin A. Persson – Department of Material Science and Engineering, University of California, Berkeley, California 94720, United States; Materials Science Division, Lawrence Berkeley National Laboratory, Berkeley, California 94720, United States; orcid.org/0000-0003-2495-5509; Email: kristinpersson@berkeley.edu

Authors

Roberta Pascazio — Department of Material Science and Engineering, University of California, Berkeley, California 94720, United States; Materials Science Division, Lawrence Berkeley National Laboratory, Berkeley, California 94720, United States; orcid.org/0009-0009-6860-6221

Qian Chen — Department of Material Science and Engineering, University of California, Berkeley, California 94720, United States; Materials Science Division, Lawrence Berkeley National Laboratory, Berkeley, California 94720, United States; Present Address: Toyota Research Institute of North America, Ann Arbor, Michigan 48105, United States; orcid.org/0009-0009-3557-0744

Haoming Howard Li — Department of Material Science and Engineering, University of California, Berkeley, California 94720, United States; Materials Science Division, Lawrence Berkeley National Laboratory, Berkeley, California 94720, United States; orcid.org/0000-0001-7450-172X

Aaron D. Kaplan – Materials Science Division, Lawrence Berkeley National Laboratory, Berkeley, California 94720, United States; Oorcid.org/0000-0003-3439-4856

Complete contact information is available at: https://pubs.acs.org/10.1021/acs.chemmater.5c00916

Author Contributions

R.P. and Q.C. contributed equally to this work. The manuscript was written through contributions of all authors.

R.P. completed the diffusion calculations, data analysis for stability and electrochemical properties and descriptor analysis, visualization, drafting, reviewing and editing of the paper. Q.C. designed and performed the screening procedure, the insertion, and the preliminary diffusion calculations, data analysis for stability and electrochemical properties, and supervised the preparation and editing of the manuscript. H.H.L. and A.D.K. carried out the supervision of the insertion and diffusion algorithms and supervised the preparation and editing. K.A.P. provided supervising and funding at all stages and editing of the manuscript. All authors have given approval to the final version of the manuscript.

Notes

The authors declare no competing financial interest.

ACKNOWLEDGMENTS

This work was intellectually led by the BEACONS Center at UT Dallas supported by the U.S. Department of Defense's Office of Industrial Base Policy and its Manufacturing Capability Expansion and investment Prioritization (MCEIP) office funding of the Batteries and Energy to Advance Commercialization and National Security (BEACONS) at the University of Texas at Dallas. Partial support was obtained from the Energy Storage Research Alliance "ESRA" (DE-AC02-06CH11357), an Energy Innovation Hub funded by the U.S. Department of Energy, Office of Science, Basic Energy Sciences. Data and workflow algorithms provided and further developed with the aid of the Materials Project, which is funded by the U.S. Department of Energy, Office of Science, Office of Basic Energy Sciences, Materials Sciences and Engineering Division, under Contract No. DE-AC02-05-CH11231: Materials Project Program KC23MP. Our research used resources of the National Energy Research Scientific Computing Center (NERSC), a Department of Energy Office of Science User Facility using NERSC award DOE-ERCAP0026371.

ABBREVIATIONS

ZIB Zn-ion battery LIB Li-ion battery

DFT density functional theory
PBA Prussian blue analogues
EDX energy-dispersive X-ray
MP Materials Project
TM transition metal

NASICON sodium superionic conductors ICSD Inorganic Crystal Structure Database (CI)-NEB (climbing-image)-nudged elastic band

AIMD ab initio molecular dynamics OER oxygen evolution reaction SHE standard hydrogen electrode

REFERENCES

- (1) Wang, L.; Zheng, J. Recent advances in cathode materials of rechargeable aqueous zinc-ion batteries. *Mater. Today Adv.* **2020**, *7*, No. 100078.
- (2) Armand, M.; Tarascon, J.-M. Building Better Batteries. *Nature* **2008**, *451*, 652–7.
- (3) Zhou, T.; Zhu, L.; Xie, L.; Han, Q.; Yang, X.; Chen, L.; Wang, G.; Cao, X. Cathode materials for aqueous zinc-ion batteries: A mini review. *J. Colloid Interface Sci.* **2022**, *605*, 828–850.
- (4) Sony Group Corporation. A Dream Comes True: The Lithium-Ion Rechargeable Battery. https://www.sony.com/en/SonyInfo/

CorporateInfo/History/SonyHistory/2-13.html (accessed June 25, 2025).

- (5) Lu, Y.; Goodenough, J. B.; Kim, Y. Aqueous Cathode for Next-Generation Alkali-Ion Batteries. *J. Am. Chem. Soc.* **2011**, *133*, 5756–5759.
- (6) Larcher, D.; Tarascon, J.-M. Towards greener and more sustainable batteries for electrical energy storage. *Nat. Chem.* **2015**, 7, 19–29.
- (7) Goodenough, J. B.; Kim, Y. Challenges for Rechargeable Li Batteries. *Chem. Mater.* **2010**, 22, 587–603.
- (8) Goodenough, J. B.; Park, K.-S. The Li-Ion Rechargeable Battery: A Perspective. J. Am. Chem. Soc. 2013, 135, 1167–1176.
- (9) Rutt, A.; Shen, J.-X.; Horton, M.; Kim, J.; Lin, J.; Persson, K. A. Expanding the Material Search Space for Multivalent Cathodes. *ACS Appl. Mater. Interfaces* **2022**, *14*, 44367–44376.
- (10) Ming, J.; Guo, J.; Xia, C.; Wang, W.; Alshareef, H. N. Zinc-ion batteries: Materials, mechanisms, and applications. *Mater. Sci. Eng., R* **2019**, *135*, 58–84.
- (11) Kundu, D.; Hosseini Vajargah, S.; Wan, L.; Adams, B.; Prendergast, D.; Nazar, L. F. Aqueous vs. nonaqueous Zn-ion batteries: consequences of the desolvation penalty at the interface. *Energy Environ. Sci.* **2018**, *11*, 881–892.
- (12) Ponrouch, A.; Bitenc, J.; Dominko, R.; Lindahl, N.; Johansson, P.; Palacin, M. Multivalent rechargeable batteries. *Energy Storage Mater.* **2019**, 20, 253–262.
- (13) Nie, C.; Wang, G.; Wang, D.; Wang, M.; Gao, X.; Bai, Z.; Wang, N.; Yang, J.; Xing, Z.; Dou, S. Recent Progress on Zn Anodes for Advanced Aqueous Zinc-Ion Batteries. *Adv. Energy Mater.* **2023**, *13*, No. 2300606.
- (14) Song, J.; Xu, K.; Liu, N.; Reed, D.; Li, X. Crossroads in the renaissance of rechargeable aqueous zinc batteries. *Mater. Today* **2021**, 45, 191–212.
- (15) Ju, Z.; Zheng, T.; Zhang, B.; Yu, G. Interfacial chemistry in multivalent aqueous batteries: fundamentals, challenges, and advances. *Chem. Soc. Rev.* **2024**, *53*, 8980–9028.
- (16) Ahn, H.; Kim, D.; Lee, M.; Nam, K. W. Challenges and possibilities for aqueous battery systems. *Commun. Mater.* **2023**, 4, No. 37.
- (17) Yang, W.; Du, X.; Zhao, J.; Chen, Z.; Li, J.; Xie, J.; Zhang, Y.; Cui, Z.; Kong, Q.; Zhao, Z.; et al. Hydrated eutectic electrolytes with ligand-oriented solvation shells for long-cycling zinc-organic batteries. *Joule* **2020**, *4*, 1557–1574.
- (18) Chang, N.; Li, T.; Li, R.; Wang, S.; Yin, Y.; Zhang, H.; Li, X. An aqueous hybrid electrolyte for low-temperature zinc-based energy storage devices. *Energy Environ. Sci.* **2020**, *13*, 3527–3535.
- (19) Hao, J.; Yuan, L.; Ye, C.; Chao, D.; Davey, K.; Guo, Z.; Qiao, S.-Z. Boosting zinc electrode reversibility in aqueous electrolytes by using low-cost antisolvents. *Angew. Chem., Int. Ed.* **2021**, *60*, 7366–7375.
- (20) Li, C.; Kingsbury, R.; Thind, A. S.; Shyamsunder, A.; Fister, T. T.; Klie, R. F.; Persson, K. A.; Nazar, L. F. Enabling selective zinc-ion intercalation by a eutectic electrolyte for practical anodeless zinc batteries. *Nat. Commun.* **2023**, *14*, No. 3067.
- (21) Shen, Y.; Liu, B.; Liu, X.; Liu, J.; Ding, J.; Zhong, C.; Hu, W. Water-in-salt electrolyte for safe and high-energy aqueous battery. *Energy Storage Mater.* **2021**, *34*, 461–474.
- (22) Tian, S.; Hwang, T.; Malakpour Estalaki, S.; Tian, Y.; Zhou, L.; Milazzo, T.; Moon, S.; Wu, S.; Jian, R.; Balkus, K., Jr; et al. A Low-Cost Quasi-Solid-State "Water-in-Swelling-Clay" Electrolyte Enabling Ultrastable Aqueous Zinc-Ion Batteries. *Adv. Energy Mater.* **2023**, *13*, No. 2300782.
- (23) Wang, Z.; Diao, J.; Burrow, J. N.; Brotherton, Z. W.; Lynd, N. A.; Henkelman, G.; Mullins, C. B. Chaotropic Salt-Aided "Water-In-Organic" Electrolyte for Highly Reversible Zinc-Ion Batteries Across a Wide Temperature Range. *Adv. Funct. Mater.* **2024**, *34*, No. 2311271.
- (24) Liu, Z.; El Abedin, S. Z.; Endres, F. Electrodeposition of zinc films from ionic liquids and ionic liquid/water mixtures. *Electrochim. Acta* **2013**, *89*, *635*–*643*.

- (25) Sownthari, K.; Suthanthiraraj, S. A. Synthesis and characterization of an electrolyte system based on a biodegradable polymer. *eXPRESS Polym. Lett.* **2013**, *7*, 495–504.
- (26) Abbott, A. P.; Barron, J. C.; Ryder, K. S. Electrolytic deposition of Zn coatings from ionic liquids based on choline chloride. *Trans. IMF* **2009**, 87, 201–207.
- (27) Han, S.-D.; Rajput, N. N.; Qu, X.; Pan, B.; He, M.; Ferrandon, M. S.; Liao, C.; Persson, K. A.; Burrell, A. K. Origin of electrochemical, structural, and transport properties in nonaqueous zinc electrolytes. *ACS Appl. Mater. Interfaces* **2016**, *8*, 3021–3031.
- (28) Senguttuvan, P.; Han, S.-D.; Kim, S.; Lipson, A. L.; Tepavcevic, S.; Fister, T. T.; Bloom, I. D.; Burrell, A. K.; Johnson, C. S. A High Power Rechargeable Nonaqueous Multivalent Zn/V 2 O 5 Battery. *Adv. Energy Mater.* **2016**, *6*, No. 1600826.
- (29) Qiu, H.; Du, X.; Zhao, J.; Wang, Y.; Ju, J.; Chen, Z.; Hu, Z.; Yan, D.; Zhou, X.; Cui, G. Zinc anode-compatible in-situ solid electrolyte interphase via cation solvation modulation. *Nat. Commun.* **2019**, *10*, No. 5374.
- (30) Naveed, A.; Yang, H.; Shao, Y.; Yang, J.; Yanna, N.; Liu, J.; Shi, S.; Zhang, L.; Ye, A.; He, B.; Wang, J. A highly reversible Zn anode with intrinsically safe organic electrolyte for long-cycle-life batteries. *Adv. Mater.* **2019**, *31*, No. 1900668.
- (31) Kim, J.; Sari, D.; Chen, Q.; Ceder, G.; Persson, K. A. Evaluating Material Design Principles for Calcium-Ion Mobility in Intercalation Cathodes. *Chem. Mater.* **2025**, *37*, 507–519.
- (32) Jun, K.; Chen, Y.; Wei, G.; Yang, X.; Ceder, G. Diffusion mechanisms of fast lithium-ion conductors. *Nat. Rev. Mater.* **2024**, *9*, 887–905.
- (33) Manthiram, A.; Goodenough, J. Lithium insertion into Fe2 (SO4) 3 frameworks. *J. Power Sources* **1989**, *26*, 403–408.
- (34) Etourneau, J.; Portier, J.; Ménil, F. The role of the inductive effect in solid state chemistry: how the chemist can use it to modify both the structural and the physical properties of the materials. *J. Alloys Compd.* **1992**, *188*, 1–7.
- (35) Liu, M.; Rong, Z.; Malik, R.; Canepa, P.; Jain, A.; Ceder, G.; Persson, K. A. Spinel compounds as multivalent battery cathodes: a systematic evaluation based on ab initio calculations. *Energy Environ. Sci.* **2015**, *8*, 964–974.
- (36) Canepa, P.; Bo, S.-H.; Sai Gautam, G.; Key, B.; Richards, W. D.; Shi, T.; Tian, Y.; Wang, Y.; Li, J.; Ceder, G. High magnesium mobility in ternary spinel chalcogenides. *Nat. Commun.* **2017**, *8*, No. 1759.
- (37) Miranda Miliante, C.; Gourley, S.; Adams, B. D.; Higgins, D.; Rubel, O. Roadmap for the Development of Transition Metal Oxide Cathodes for Rechargeable Zinc-Ion Batteries. *J. Phys. Chem. C* **2024**, *128*. 17261–17273.
- (38) Gautam, G. S.; Canepa, P.; Malik, R.; Liu, M.; Persson, K.; Ceder, G. First-principles evaluation of multi-valent cation insertion into orthorhombic V2O5. *Chem. Commun.* **2015**, *51*, 13619–13622.
- (39) Liu, M.; Jain, A.; Rong, Z.; Qu, X.; Canepa, P.; Malik, R.; Ceder, G.; Persson, K. A. Evaluation of sulfur spinel compounds for multivalent battery cathode applications. *Energy Environ. Sci.* **2016**, *9*, 3201–3209.
- (40) Rong, Z.; Malik, R.; Canepa, P.; Sai Gautam, G.; Liu, M.; Jain, A.; Persson, K.; Ceder, G. Materials Design Rules for Multivalent Ion Mobility in Intercalation Structures. *Chem. Mater.* **2015**, *27*, 6016–6021.
- (41) Guo, X.; Zhou, J.; Bai, C.; Li, X.; Fang, G.; Liang, S. Zn/MnO2 battery chemistry with dissolution-deposition mechanism. *Mater. Today Energy* **2020**, *16*, No. 100396.
- (42) Zhang, G.; Wu, T.; Zhou, H.; Jin, H.; Liu, K.; Luo, Y.; Jiang, H.; Huang, K.; Huang, L.; Zhou, J. Rich Alkali Ions Preintercalated Vanadium Oxides for Durable and Fast Zinc-Ion Storage. ACS Energy Lett. 2021, 6, 2111–2120.
- (43) Li, H. H.; Shen, J.-X.; Persson, K. A. A rapid lithium-ion cathode discovery pipeline and its exemplary application. *Energy Adv.* **2024**, *3*, 255–262.

- (44) Singh, A. K.; Zhou, L.; Shinde, A.; Suram, S. K.; Montoya, J. H.; Winston, D.; Gregoire, J. M.; Persson, K. A. Electrochemical stability of metastable materials. *Chem. Mater.* **2017**, *29*, 10159–10167.
- (45) Ong, S. P.; Wang, L.; Kang, B.; Ceder, G. Li- Fe- P- O2 phase diagram from first principles calculations. *Chem. Mater.* **2008**, *20*, 1798–1807.
- (46) Jain, A.; Ong, S. P.; Hautier, G.; Chen, W.; Richards, W. D.; Dacek, S.; Cholia, S.; Gunter, D.; Skinner, D.; Ceder, G.; Persson, K. A. Commentary: The Materials Project: A materials genome approach to accelerating materials innovation. *APL Mater.* **2013**, *1*, No. 011002.
- (47) Horton, M. K.; Huck, P.; Yang, R. X.; Munro, J. M.; Dwaraknath, S.; Ganose, A. M.; Kingsbury, R. S.; Wen, M.; Shen, J. X.; Mathis, T. S.; et al. Accelerated data-driven materials science with the Materials Project. *Nat. Mater.* **2025**, 1–11.
- (48) Hautier, G.; Ong, S. P.; Jain, A.; Moore, C. J.; Ceder, G. Accuracy of density functional theory in predicting formation energies of ternary oxides from binary oxides and its implication on phase stability. *Phys. Rev. B* **2012**, *85*, No. 155208.
- (49) Sun, W.; Dacek, S. T.; Ong, S. P.; Hautier, G.; Jain, A.; Richards, W. D.; Gamst, A. C.; Persson, K. A.; Ceder, G. The thermodynamic scale of inorganic crystalline metastability. *Sci. Adv.* **2016**, *2*, No. e1600225.
- (50) Shen, J.-X.; Horton, M.; Persson, K. A. A charge-density-based general cation insertion algorithm for generating new Li-ion cathode materials. *npj Comput. Mater.* **2020**, *6*, No. 161.
- (51) Hannah, D. C.; Sai Gautam, G.; Canepa, P.; Ceder, G. On the Balance of Intercalation and Conversion Reactions in Battery Cathodes. *Adv. Energy Mater.* **2018**, *8*, No. 1800379.
- (52) Gunter, D.; Cholia, S.; Jain, A.; Kocher, M.; Persson, K.; Ramakrishnan, L.; Ong, S. P.; Ceder, G. In *Community accessible datastore of high-throughput calculations: experiences from the Materials Project*, 2012 SC Companion: High Performance Computing, Networking Storage and Analysis, 2012; pp 1244–1251.
- (53) Persson, K. A.; Waldwick, B.; Lazic, P.; Ceder, G. Prediction of solid-aqueous equilibria: Scheme to combine first-principles calculations of solids with experimental aqueous states. *Phys. Rev. B: Condens. Matter Mater. Phys.* **2012**, *85*, No. 235438.
- (54) Ong, S. P.; Richards, W. D.; Jain, A.; Hautier, G.; Kocher, M.; Cholia, S.; Gunter, D.; Chevrier, V. L.; Persson, K. A.; Ceder, G. Python Materials Genomics (pymatgen): A robust, open-source python library for materials analysis. *Comput. Mater. Sci.* **2013**, *68*, 314–319.
- (55) Shen, J.-X.; Li, H. H.; Rutt, A.; Horton, M. K.; Persson, K. A. Topological graph-based analysis of solid-state ion migration. *npj Comput. Mater.* **2023**, *9*, No. 99.
- (56) Koistinen, O.-P.; Dagbjartsdóttir, F. B.; Ásgeirsson, V.; Vehtari, A.; Jónsson, H. Nudged elastic band calculations accelerated with Gaussian process regression. *J. Chem. Phys.* **2017**, *147*, No. 152720.
- (57) Rong, Z.; Kitchaev, D.; Canepa, P.; Huang, W.; Ceder, G. An efficient algorithm for finding the minimum energy path for cation migration in ionic materials. *J. Chem. Phys.* **2016**, *145*, No. 074112.
- (\$8) Mathew, K.; Montoya, J. H.; Faghaninia, A.; et al. Atomate: A high-level interface to generate, execute, and analyze computational materials science workflows. *Comput. Mater. Sci.* **2017**, *139*, 140–152.
- (59) Ganose, A. M.; Sahasrabuddhe, H.; Asta, M.; Beck, K.; Biswas, T.; Bonkowski, A.; Bustamante, J.; Chen, X.; Chiang, Y.; Chrzan, D. C.; et al. Atomate2: Modular workflows for materials science. *Digital Discovery* **2025**, DOI: 10.1039/d5dd00019j.
- (60) Mills, G.; Jónsson, H.; Schenter, G. K. Reversible work transition state theory: application to dissociative adsorption of hydrogen. *Surf. Sci.* **1995**, 324, 305–337.
- (61) Henkelman, G.; Uberuaga, B. P.; Jónsson, H. A climbing image nudged elastic band method for finding saddle points and minimum energy paths. *J. Chem. Phys.* **2000**, *113*, 9901–9904.
- (62) Suo, L.; Borodin, O.; Gao, T.; Olguin, M.; Ho, J.; Fan, X.; Luo, C.; Wang, C.; Xu, K. "Water-in-salt" electrolyte enables high-voltage aqueous lithium-ion chemistries. *Science* **2015**, *350*, 938–943.

- (63) Borodin, O.; Self, J.; Persson, K. A.; Wang, C.; Xu, K. Uncharted waters: super-concentrated electrolytes. *Joule* **2020**, *4*, 69–100
- (64) Hautier, G.; Jain, A.; Ong, S. P.; Kang, B.; Moore, C.; Doe, R.; Ceder, G. Phosphates as lithium-ion battery cathodes: an evaluation based on high-throughput ab initio calculations. *Chem. Mater.* **2011**, 23, 3495–3508.
- (65) Li, W.; Song, B.; Manthiram, A. High-voltage positive electrode materials for lithium-ion batteries. *Chem. Soc. Rev.* **2017**, *46*, 3006–3059.
- (66) Ni, Q.; Bai, Y.; Wu, F.; Wu, C. Polyanion-type electrode materials for sodium-ion batteries. *Adv. Sci.* **2017**, *4*, No. 1600275.
- (67) Liu, C.; Neale, Z. G.; Cao, G. Understanding electrochemical potentials of cathode materials in rechargeable batteries. *Mater. Today* **2016**, *19*, 109–123.
- (68) Li, H. H.; Chen, Q.; Ceder, G.; Persson, K. A. Voltage Mining for (De) lithiation-Stabilized Cathodes and a Machine Learning Model for Li-Ion Cathode Voltage. *ACS Appl. Mater. Interfaces* **2024**, *16*, 69379–69387.
- (69) Fedotov, S. S.; Khasanova, N. R.; Samarin, A. S.; Drozhzhin, O. A.; Batuk, D.; Karakulina, O. M.; Hadermann, J.; Abakumov, A. M.; Antipov, E. V. AVPO4F (A= Li, K): a 4 V cathode material for highpower rechargeable batteries. *Chem. Mater.* **2016**, *28*, 411–415.
- (70) Mueller, T.; Hautier, G.; Jain, A.; Ceder, G. Evaluation of tavorite-structured cathode materials for lithium-ion batteries using high-throughput computing. *Chem. Mater.* **2011**, *23*, 3854–3862.
- (71) Nisar, U.; Shakoor, R.; Essehli, R.; Amin, R.; Orayech, B.; Ahmad, Z.; Kumar, P. R.; Kahraman, R.; Al-Qaradawi, S.; Soliman, A. Sodium intercalation/de-intercalation mechanism in Na4MnV (PO4) 3 cathode materials. *Electrochim. Acta* **2018**, *292*, 98–106.
- (72) Li, G.; Yang, Z.; Jiang, Y.; Jin, C.; Huang, W.; Ding, X.; Huang, Y. Towards polyvalent ion batteries: A zinc-ion battery based on NASICON structured Na3V2 (PO4) 3. *Nano Energy* **2016**, 25, 211–217.
- (73) Canepa, P.; Sai Gautam, G.; Hannah, D. C.; Malik, R.; Liu, M.; Gallagher, K. G.; Persson, K. A.; Ceder, G. Odyssey of multivalent cathode materials: open questions and future challenges. *Chem. Rev.* **2017**, *117*, 4287–4341.
- (74) Liang, Y.; Wen, K.; Mao, Y.; Liu, Z.; Zhu, G.; Yang, F.; He, W. Shape and Size Control of LiFePO4 for High-Performance Lithium-Ion Batteries. *ChemElectroChem* **2015**, *2*, 1227–1237.
- (75) Masquelier, C.; Padhi, A.; Nanjundaswamy, K.; Goodenough, J. New cathode materials for rechargeable lithium batteries: the 3-D framework structures Li3Fe2 (XO4) 3 (X= P, As). *J. Solid State Chem.* **1998**, 135, 228–234.
- (76) Masquelier, C.; Croguennec, L. Polyanionic (phosphates, silicates, sulfates) frameworks as electrode materials for rechargeable Li (or Na) batteries. *Chem. Rev.* **2013**, *113*, 6552–6591.
- (77) Zhao, X.; Zhang, Z.; Zhang, X.; Tang, B.; Xie, Z.; Zhou, Z. Computational screening and first-principles investigations of NASICON-type Li x M 2 (PO 4) 3 as solid electrolytes for Li batteries. *J. Mater. Chem. A* **2018**, *6*, 2625–2631.
- (78) Zhang, Z.; Zou, Z.; Kaup, K.; Xiao, R.; Shi, S.; Avdeev, M.; Hu, Y.-S.; Wang, D.; He, B.; Li, H.; et al. Correlated migration invokes higher Na+-ion conductivity in NaSICON-type solid electrolytes. *Adv. Energy Mater.* **2019**, *9*, No. 1902373.
- (79) Gao, H.; Seymour, I. D.; Xin, S.; Xue, L.; Henkelman, G.; Goodenough, J. B. Na3MnZr (PO4) 3: a high-voltage cathode for sodium batteries. *J. Am. Chem. Soc.* **2018**, *140*, 18192–18199.
- (80) Patoux, S.; Rousse, G.; Leriche, J.-B.; Masquelier, C. Structural and electrochemical studies of rhombohedral Na2TiM (PO4) 3 and Li1. 6Na0. 4TiM (PO4) 3 (M= Fe, Cr) phosphates. *Chem. Mater.* 2003, 15, 2084–2093.
- (81) Ding, J.; Gao, H.; Ji, D.; Zhao, K.; Wang, S.; Cheng, F. Vanadium-based cathodes for aqueous zinc-ion batteries: from crystal structures, diffusion channels to storage mechanisms. *J. Mater. Chem.* A 2021, 9, 5258–5275.

- (82) Van der Ven, A.; Bhattacharya, J.; Belak, A. A. Understanding Li diffusion in Li-intercalation compounds. *Acc. Chem. Res.* **2013**, *46*, 1216–1225
- (83) Xu, B.; Meng, S. Factors affecting Li mobility in spinel LiMn2O4—A first-principles study by GGA and GGA+ U methods. *J. Power Sources* **2010**, 195, 4971–4976.
- (84) Lu, W.; Wang, J.; Sai Gautam, G.; Canepa, P. Searching ternary oxides and chalcogenides as positive electrodes for calcium batteries. *Chem. Mater.* **2021**, *33*, 5809–5821.
- (85) Urban, A.; Seo, D.-H.; Ceder, G. Computational understanding of Li-ion batteries. *npj Comput. Mater.* **2016**, *2*, No. 16002.
- (86) Kang, K.; Ceder, G. Factors that affect Li mobility in layered lithium transition metal oxides. *Phys. Rev. B: Condens. Matter Mater. Phys.* **2006**, 74, No. 094105.
- (87) Ahsan, Z.; Cai, Z.; Wang, S.; Moin, M.; Wang, H.; Liu, D.; Ma, Y.; Song, G.; Wen, C. Recent Development of Phosphate Based Polyanion Cathode Materials for Sodium-Ion Batteries. *Adv. Energy Mater.* **2024**, *14*, No. 2400373.
- (88) Okada, S.; Ueno, M.; Uebou, Y.; Yamaki, J.-i. Fluoride phosphate Li2CoPO4F as a high-voltage cathode in Li-ion batteries. *J. Power Sources* **2005**, *146*, 565–569.
- (89) Schoiber, J.; Berger, R. J.; Bernardi, J.; Schubert, M.; Yada, C.; Miki, H.; Hüsing, N. Straightforward Solvothermal Synthesis toward Phase Pure Li2CoPO4F. *Cryst. Growth Des.* **2016**, *16*, 4999–5005.
- (90) Hadermann, J.; Abakumov, A. M.; Turner, S.; Hafideddine, Z.; Khasanova, N. R.; Antipov, E. V.; Van Tendeloo, G. Solving the structure of Li ion battery materials with precession electron diffraction: Application to Li2CoPO4F. *Chem. Mater.* **2011**, 23, 3540–3545.
- (91) Pérez-Vicente, C.; Alcántara, R. New perspectives on the multianion approach to adapt electrode materials for lithium and post-lithium batteries. *Phys. Chem. Chem. Phys.* **2023**, 25, 15600–15623.
- (92) Fedotov, S. S.; Kabanov, A. A.; Kabanova, N. A.; Blatov, V. A.; Zhugayevych, A.; Abakumov, A. M.; Khasanova, N. R.; Antipov, E. V. Crystal structure and Li-ion transport in Li2CoPO4F high-voltage cathode material for Li-ion batteries. *J. Phys. Chem. C* **2017**, *121*, 3194–3202.
- (93) Kubota, K.; Yokoh, K.; Yabuuchi, N.; Komaba, S. Na2CoPO4F as a high-voltage electrode material for Na-ion batteries. *Electrochemistry* **2014**, *82*, 909–911.
- (94) Piffard, Y.; Oyetola, S.; Verbaere, A.; Tournoux, M. Synthesis, thermal stability, and crystal structure of antimony (V) phosphate SbOPO4. *J. Solid State Chem.* **1986**, *63*, 81–85.
- (95) Amos, T.; Sleight, A. Negative thermal expansion in orthorhombic NbOPO4. *J. Solid State Chem.* **2001**, *160*, 230–238.
- (96) Leclaire, A.; Chahboun, N.; Groult, D.; Raveau, B. The crystal structure of β -NbPO5. *Z. Kristallogr. Cryst. Mater.* **1986**, 177, 277–286.
- (97) Lu, M. Y.; Badway, F.; Kim, J. R.; Amatucci, G. G. Investigation of Physical and Electrochemical Properties of β -Ta x Nb1-x PO5 as an Electrode Material for Lithium Batteries. *Chem. Mater.* **2016**, 28, 2949–2961.
- (98) Chernova, N. A.; Hidalgo, M. F. V.; Kaplan, C.; Lee, K.; Buyuker, I.; Siu, C.; Wen, B.; Ding, J.; Zuba, M.; Wiaderek, K. M.; et al. Vanadyl phosphates AxVOPO4 (A= Li, Na, K) as multielectron cathodes for alkali-ion batteries. *Adv. Energy Mater.* **2020**, *10*, No. 2002638.
- (99) Ma, S.; Jiang, T.; Deng, J.; Zhang, Q.; Ou, Y.; Liu, X.; Lin, C.; Wang, K.; Zhao, X. VPO5: an all-climate lithium-storage material. *Energy Storage Mater.* **2022**, *46*, 366–373.
- (100) Sari, D.; Rutt, A.; Kim, J.; Chen, Q.; Hahn, N. T.; Kim, H.; Persson, K. A.; Ceder, G. Alkali-Ion-Assisted Activation of ε -VOPO4 as a Cathode Material for Mg-Ion Batteries. *Adv. Sci.* **2024**, *11*, No. 2307838.
- (101) Zhao, D.; Pu, X.; Tang, S.; Ding, M.; Zeng, Y.; Cao, Y.; Chen, Z. δ -VOPO 4 as a high-voltage cathode material for aqueous zinc-ion batteries. *Chem. Sci.* **2023**, *14*, 8206–8213.

(102) He, G.; Huq, A.; Kan, W. H.; Manthiram, A. β -NaVOPO4 obtained by a low-temperature synthesis process: a new 3.3 V cathode for sodium-ion batteries. *Chem. Mater.* **2016**, *28*, 1503–1512.

- (103) Gopal, R.; Calvo, C. Crystal structure of β VPO5. *J. Solid State Chem.* **1972**, *5*, 432–435.
- (104) Aparicio, P. A.; Dawson, J. A.; Islam, M. S.; De Leeuw, N. H. Computational study of NaVOPO4 polymorphs as cathode materials for Na-ion batteries: Diffusion, electronic properties, and cation-doping behavior. *J. Phys. Chem. C* **2018**, *122*, 25829–25836.
- (105) Liu, Y.; Li, J.; Shen, Q.; Zhang, J.; He, P.; Qu, X.; Liu, Y. Advanced characterizations and measurements for sodium-ion batteries with NASICON-type cathode materials. *eScience* **2022**, *2*, 10–31.
- (106) Zhou, Y.; Xu, G.; Lin, J.; Zhang, Y.; Fang, G.; Zhou, J.; Cao, X.; Liang, S. Reversible Multielectron Redox Chemistry in a NASICON-Type Cathode toward High-Energy-Density and Long-Life Sodium-Ion Full Batteries. *Adv. Mater.* **2023**, *35*, No. 2304428.
- (107) Wang, J.; He, T.; Yang, X.; Cai, Z.; Wang, Y.; Lacivita, V.; Kim, H.; Ouyang, B.; Ceder, G. Design principles for NASICON super-ionic conductors. *Nat. Commun.* **2023**, *14*, No. 5210.
- (108) Leclaire, A.; Borel, M.-M.; Grandin, A.; Raveau, B. A mixed-valence niobium phosphate with an empty nasicon structure: Nb2 (PO4) 3. Cryst. Struct. Commun. 1989, 45, 699–701.
- (109) Patra, B.; Kumar, K.; Deb, D.; Ghosh, S.; Gautam, G. S.; Senguttuvan, P. Unveiling a high capacity multi-redox (Nb 5+/Nb 4+/Nb 3+) NASICON-Nb 2 (PO 4) 3 anode for Li-and Na-ion batteries. *J. Mater. Chem. A* **2023**, *11*, 8173–8183.
- (110) Brown, I. D. What factors determine cation coordination numbers? Acta Crystallogr., Sect. B: Struct. Sci. 1988, 44, 545–553.
- (111) Momma, K.; Izumi, F. VESTA 3 for three-dimensional visualization of crystal, volumetric and morphology data. *J. Appl. Crystallogr.* **2011**, *44*, 1272–1276.
- (112) Pan, H.; Ganose, A. M.; Horton, M.; Aykol, M.; Persson, K. A.; Zimmermann, N. E.; Jain, A. Benchmarking coordination number prediction algorithms on inorganic crystal structures. *Inorg. Chem.* **2021**, *60*, 1590–1603.
- (113) Van der Ven, A.; Ceder, G. Lithium Diffusion in Layered LixCoO2. Electrochem. Solid-State Lett. 2000, 3, 301.
- (114) Van der Ven, A.; Ceder, G. Lithium diffusion mechanisms in layered intercalation compounds. *J. Power Sources* **2001**, 97–98, 529–531.
- (115) Kang, K.; Meng, Y. S.; Breger, J.; Grey, C. P.; Ceder, G. Electrodes with high power and high capacity for rechargeable lithium batteries. *Science* **2006**, *311*, 977–980.
- (116) Jang, Y.-I.; Neudecker, B. J.; Dudney, N. J. Lithium diffusion in LixCoO2 (0.45 < x < 0.7) intercalation cathodes. *Electrochem. Solid-State Lett.* **2001**, *4*, A74.

